A model incorporating damage evolution to predict the penetration behaviour of a ceramic target subjected to the long projectile impact

Zhiyong Wang [a], Peifeng Li [b,*]

[a] School of Mechatronical Engineering, Beijing Institute of Technology, Beijing, China

[b] James Watt School of Engineering, University of Glasgow, Glasgow, UK

[*] Corresponding author's email: peifeng.li@glasgow.ac.uk (P. Li); Tel: +44 141 330 2703.

Abstract

Predicting the ballistic performance of a ceramic armour composite system requires the accurate constitutive formulation of the ceramic target material. In this study, the analytical spherical cavity expansion model was modified to simulate the penetration process of a ceramic target impacted by a long projectile, and then validated by the data in the literature. Specifically a damage evolution parameter that characterises the modulus degradation in the ceramic was proposed and incorporated into the model. It was found that the prediction is more accurate when the model includes damage evolution. Parametric modelling further reveals that the properties of the projectile and target materials have a significant effect on the penetration response. The target resistance is sensitive to the damage evolution, especially in the ceramic of higher dynamic compressive strength and lower tensile strength. The modified model

enables the selection of target materials for penetration resistance in terms of not just strength but also toughness.

Keywords: Ceramics; Damage evolution; Ballistic performance; Penetration velocity; Target resistance.

1 Introduction

As the key component in lightweight layered armour composites, ceramic materials provide the high resistance and energy dissipation capacity against penetrating impact. The ballistic performance of such armour ceramics has been studied experimentally and numerically under a range of small calibre ammunition impact [1-6]. The design and optimisation of the armour composite system require the accurate prediction of the penetration behaviour of ceramic materials subjected to high speed impact loading.

Numerous research activities have been performed in the past decades to investigate the correlation between material properties of ceramics and their dynamic response including the ballistic performance in high strain rate conditions [7-16]. The dynamic behaviour of ceramic materials is significantly affected by their properties such as hardness, elastic modulus, fracture toughness and failure probability [10, 17-24]. The shear strength increases with the confining pressure at high loading rates due to the shear-induced dilatation [3]. The penetration resistance could be approximately 2.5 times the dynamic strength of ceramics [15, 25]. The penetration velocity, independent of the projectile diameter, varies linearly with the impact velocity in the higher impact velocity range, but nonlinearly at the relatively lower impact velocity [26, 27]. The complicated penetration process involves a wide range of physical phenomena such as shock wave propagation, damage evolution, plugging process, melting and phase transformation [28, 29]. Therefore, simplification by only

considering some key factors is more realistic and often made to evaluate the ballistic performance of ceramics subjected to the projectile impact.

Early analytical work on the penetration behaviour used a modified hydrodynamic theory incorporating the strength effect to estimate the deceleration process of the projectile, but the model was only suitable for metal targets [30]. A Taylor ballistic impact model was then developed to determine the deformation and mass loss of the projectile, considering both the erosion and deformation mechanisms [31]. The erosion of both the projectile and ceramic target has been integrated into a 1D approach to simulate the ceramic armour composite failure using a lumped mass scheme [32]. The agreement of this model with experimental results enabled the investigation of the penetration behaviour of ceramic targets. The penetration resistance and penetration velocity, which are difficult to measure directly, are the two key parameters to evaluate the ability of a target to resist penetration. Most of the analytical models to predict these penetration parameters in ceramic targets subjected to a long rod impact are empirical or experimentally-based [8, 33-37]. Among them, the cavity expansion theory has been used to analytically relate the ceramic target resistance to the projectile velocity [13, 29, 36, 37]. The constitutive model of the ceramic material was formulated by a linear elastic response [13] or a simplified yield surface [37]. However, the elastic modulus of brittle ceramic materials usually degrades with damage evolution at high strain rates [5, 6]. It is thus necessary to

incorporate such material degradation due to damage evolution into the material model to simulate the penetration process.

The aim of this study is to develop a modified spherical cavity expansion model to determine the penetration behaviour of a ceramic target subjected to long rod projectile impact. A damage evolution function was proposed to characterise the modulus degradation in the cracked region. The model was validated with the experimental and numerical data available in the literature [15, 38]. The penetration behaviour was analysed as a function of the properties of both projectile and target materials and the damage evolution parameter. The model was finally used to estimate the important penetration variables including penetration resistance, penetration velocity, crater diameter and penetration depth.

2 Mathematical model

Fig. 1 shows the long projectile penetration process through an infinite ceramic target with an initial projectile impact velocity v_p. The penetration velocity u is defined as the projectile/target interfacial velocity at the time the target is fractured and the projectile starts to penetrate into the target. The response in a semi-infinite ceramic target can be characterised by five regions starting from the centre: the cavity, comminuted, cracked, elastic and intact regions (Fig. 2) [39]. This section describes the analytical model that is based on the spherical cavity expansion theory and

incorporates the modulus degradation due to damage evolution in the target material during the penetration process.

2.1 Constitutive model in response regions

Fig. 2(b) schematically illustrates the spherical response regions in a ceramic target and the key dimensions from the centre to the interfaces. In particular, h, a , c and b are the radius to the cavity/comminuted, comminuted/cracked, cracked/elastic and elastic/intact interfaces, respectively. Given the spherical symmetry of stress field, the boundary conditions between two adjacent response regions can be expressed in polar coordinates (referred to as the distance r and the angle θ):

- At the stress-free boundary between the intact and elastic regions:

$$\sigma_{\mathrm{r}}\big|_{r=b} = 0 \tag{1}$$

- At the interface between the elastic and cracked regions:

$$\sigma_{\theta}\big|_{r=c} = \sigma_{\mathrm{f}} \tag{2}$$

- At the boundary between the cracked and comminuted regions:

$$\sigma_{\mathrm{r}}\big|_{r=a} = -Y_{\mathrm{t}} \tag{3}$$

where σ_{r} is the radial stress, σ_{θ} is the hoop stress, σ_{f} is the tensile strength of the ceramic target, Y_{t} is the compressive strength of the target.

2.1.1 Elastic region (c<r<b)

With the assumption of a steady state penetration process, the inertia effect can be neglected in the derivation. The equilibrium equation for the elastic region in polar coordinates can be given as [13]:

$$\frac{d\sigma_{\mathrm{r}}}{dr}+2\frac{\sigma_{\mathrm{r}}-\sigma_{\theta}}{r}=0 \tag{4}$$

The radial (ε_{r}) and hoop (ε_{θ}) strains can be related to the radial displacement u_{r}:

$$\varepsilon_{\mathrm{r}}=\frac{du_{\mathrm{r}}}{dr},\quad \varepsilon_{\theta}=\frac{u_{\mathrm{r}}}{r} \tag{5}$$

The constitutive equations of the ceramic in the elastic region are thus in the form of:

$$\varepsilon_{\mathrm{r}}=\frac{1}{E}\left(\sigma_{\mathrm{r}}-2\nu\sigma_{\theta}\right) \tag{6}$$

$$\varepsilon_{\theta}=\frac{1}{E}\left[(1-\nu)\sigma_{\theta}-\nu\sigma_{\mathrm{r}}\right] \tag{7}$$

where E is the initial elastic modulus and ν is the Poisson's ratio. The stresses (σ_{r}, σ_{θ}) and the radial displacement (u_{r}) can be calculated based on Eqs. (4–7) and boundary conditions Eqs (1,2).

$$u_{\mathrm{r}}=\left(\frac{\sigma_{\mathrm{f}}}{2E}\right)\left[2(1-2\nu)r+(1+\nu)\frac{b^3}{r^2}\right]\Big/\left(1+\frac{b^3}{2c^3}\right) \tag{8}$$

$$\sigma_{\mathrm{r}}=\sigma_{\mathrm{f}}\left(1-\frac{b^3}{r^3}\right)\Big/\left(1+\frac{b^3}{2c^3}\right) \tag{9}$$

$$\sigma_{\theta}=\sigma_{\mathrm{f}}\left(1+\frac{b^3}{2r^3}\right)\Big/\left(1+\frac{b^3}{2c^3}\right) \tag{10}$$

2.1.2 Cracked region (a<r<c): a model incorporating the damage evolution

In the cracked region, the radial cracks of different sizes form when the hoop stress reaches the material tensile limit σ_f. The cracked ceramic material is thus considered to be in a radially uniaxial stress state (i.e., the hoop stress $\sigma_\theta = 0$). The stress equilibrium can be simplified by:

$$\frac{d\sigma_r}{dr} + 2\frac{\sigma_r}{r} = 0 \tag{11}$$

Applying the boundary condition at the cracked/comminuted interface Eq. (3) to Eq. (11) results in the distribution of the radial stress σ_r along the radius r.

$$\sigma_r = -\frac{Y_t a^2}{r^2} \tag{12}$$

With the consideration of stress continuity at the elastic/cracked region boundary, combining Eq. (9) and Eq. (12) gives the relation between a and c.

$$\left(\frac{a}{c}\right)^2 = -\frac{\sigma_f}{Y_t}\left(1-\frac{b^3}{c^3}\right)\Bigg/\left(1+\frac{b^3}{2c^3}\right) \tag{13}$$

The previous experiments demonstrated that dynamic fragmentation of ceramic materials is sensitive to strain rates [6]. Higher strain rates lead to smaller fragment sizes. The ceramic specimen recovered after plate impact testing revealed that within the cracked region, large radial cracks are the majority while small hoop cracks can only be found near the cracked/comminuted interface (Fig. 2(a)). The damage in the cracked region increases as the distance to the target centre decreases. The damage evolution renders material degradation and lowers the resistance to deformation.

Therefore, the material degradation due to damage evolution should be taken into account in the constitutive model in the cracked region.

Denoual and Hild [17] proposed a statistic scalar function in the exponential form to describe the degradation of brittle materials such as ceramics due to dynamic damage and fragmentation. In this study, the damage in the cracked region is quantified as an exponential function of the distance r,

$$D = 1 - \exp\left[k\left(1 - \frac{c}{r} \right) \right] \tag{14}$$

where k is the damage evolution parameter. The exponential form satisfies the following conditions.

$$\begin{cases} D = 0 & r = c \\ 0 < D < 1 & a \le r < c \end{cases} \tag{15}$$

The degraded elastic modulus is then assumed to be $E_{\mathrm{D}} = E\,(1–D)$. The stress–strain relation in the region can thus be written.

$$\sigma_{\mathrm{r}} = E_{\mathrm{D}} \frac{du_{\mathrm{r}}}{dr} = E \cdot \exp\left[k\left(1 - \frac{c}{r} \right) \right] \frac{du_{\mathrm{r}}}{dr} \tag{16}$$

When the damage effect is ignored (i.e., $k = 0$), Eq. (16) represents the linear elastic behaviour. Given the displacement continuity at the elastic/cracked interface ($r = c$), the radial displacement can be derived.

$$u_{\mathrm{r}} = \frac{\sigma_{\mathrm{f}}}{2E}\left[2(1-2\nu)c + (1+\nu)\frac{b^3}{c^2} \right] \Bigg/ \left(1 + \frac{b^3}{2c^3} \right) + \frac{Y_{\mathrm{t}} a^2}{Eck}\left\{ \exp\left[k\left(\frac{c}{r} - 1 \right) \right] - 1 \right\} \tag{17}$$

2.1.3 Comminuted region ($h<r<a$)

In this region, the comminuted ceramic can be modelled as a Mohr-Coulomb material [14]. This model describes the pressure-dependent shear strength of both intact and failed materials. The comminuted material is not subjected to any shear stress without lateral confinement (pressure). The shear stress τ can be related to the hydrostatic pressure P_{hyd} using the pressure-shear coefficient λ_{l}: $\tau = \lambda_{\text{l}} P_{\text{hyd}}$, namely, $\frac{(\sigma_{\text{r}} - \sigma_{\theta})}{2} = \lambda_{\text{l}} \frac{(\sigma_{\text{r}} + 2\sigma_{\theta})}{3}$. The equilibrium equation in the comminuted region is then simplified:

$$\frac{d\sigma_{\text{r}}}{dr} + 2\alpha \frac{\sigma_{\text{r}}}{r} = 0 \tag{18}$$

where $\alpha = 6\lambda_{\text{l}}/(3+4\ \lambda_{\text{l}})$. The pressure-shear coefficient can be calculated by $\lambda_{\text{l}} = 3\mu/(3–4\mu)$ in which μ is the normal stress to shear stress coefficient and can be determined experimentally (μ = 0.15 to 0.25 for brittle materials [10, 14]). The radial stress can thus be derived from Eq. (18) and the boundary condition Eq. (3).

$$\sigma_{\text{r}} = -Y_{\text{t}} \left(\frac{a}{r} \right)^{2\alpha} \tag{19}$$

2.2 Determination of penetration variables in the ceramic target

2.2.1 Penetration resistance

The penetration resistance of the ceramic target, also called target resistance R_{t}, is defined as the absolute value of the radial stress at the comminuted/cavity boundary. Letting $r = h$ in Eq. (19) gives,

$$R_{\mathrm{t}} = Y_{\mathrm{t}}\left(\frac{a}{h}\right)^{2\alpha} \tag{20}$$

Based on the mass conservation in Eulerian coordinates [36, 40], h and a can be related using the radial displacement $u_{\mathrm{r}}(a)$,

$$\frac{1}{3}\left(\frac{h}{a}\right)^{3} = \frac{u_{\mathrm{r}}\mid_{r=a}}{a} \tag{21}$$

Note that the ceramic target material is assumed incompressible in the derivation and the higher order terms in $u_{\mathrm{r}}(a)$ are neglected. In terms of displacement continuity for u_{r} at $r= a$ using Eq. (17), the ratio of h/a can be calculated.

$$\frac{1}{3}\left(\frac{h}{a}\right)^{3} = \frac{\sigma_{\mathrm{f}}}{2Ea}\left[2(1-2\nu)c+(1+\nu)\frac{b^{3}}{c^{2}}\right]\Bigg/\left(1+\frac{b^{3}}{2c^{3}}\right)+\frac{Y_{\mathrm{t}}a}{Eck}\left\{\exp\left[k\left(\frac{c}{a}-1\right)\right]-1\right\} \tag{22}$$

For an infinite target, the penetration resistance can be determined by combining Eqs. (13,20,22) and letting $b\to\infty$.

$$R_{\mathrm{t}} = Y_{\mathrm{t}}\left\{\frac{E/(3Y_{\mathrm{t}})}{(1+\nu)\sqrt{\sigma_{\mathrm{f}}/(2Y_{\mathrm{t}})}+1/k\cdot\sqrt{2\sigma_{\mathrm{f}}/Y_{\mathrm{t}}}\left\{\exp\left[k\left(\sqrt{\frac{Y_{\mathrm{t}}}{2\sigma_{\mathrm{f}}}}-1\right)\right]-1\right\}}\right\}^{2\alpha/3} \tag{23}$$

2.2.2 Penetration velocity

The penetration process of a projectile with a high velocity into a target can be quantitatively described by the Bernoulli equation [15, 29, 36],

$$\frac{1}{2}\rho_{p}\left(v_{p}-u\right)^{2}+Y_{p} = \frac{1}{2}\rho_{t}u^{2}+R_{t} \tag{24}$$

where ρ_p is the projectile density, ρ_t is the target density, v_p is the initial impact velocity of the projectile, u is the interfacial penetration velocity at which the projectile starts to penetrate into the target, Y_p is the dynamic strength of the projectile, and R_t is the target resistance as calculated by Eq. (23). Therefore, the penetration velocity can be determined using the given material properties of both the target and projectile.

$$u = \frac{v_p}{1-\rho_t/\rho_p}\left(1-\sqrt{\rho_t/\rho_p+\left(1-\rho_t/\rho_p\right)\frac{2\left(R_t-Y_p\right)}{\rho_p v_p^2}}\right) \tag{25}$$

2.2.3 Crater diameter

The impact process by a rod projectile usually results in an approximately circular depression in the target surface. The diameter of the crater is another indicator for the penetration ability of the projectile and the impact resistance of the target. To evaluate the crater diameter, the initial stagnation pressure p_0 is first determined by the axial pressure.

$$p_0 = \frac{1}{2}\rho_p (v_p-u)^2 + Y_p = \frac{1}{2}\rho_t u^2 + R_t \tag{26}$$

The transient stagnation pressure p is equal to the sum of both the dynamic and static pressures of the ceramic target,

$$p = \frac{1}{2}\rho_t u_c^2 + R_t \tag{27}$$

where u_c is the crater growth velocity in the radial direction. The relation between p and p_0 can be quantified using the projectile diameter D_0 and the crater diameter D_c.

$$p = \frac{D_0^2}{D_c^2} p_0 \tag{28}$$

Therefore, the radial crater growth velocity u_c can be calculated in the following equations,

$$\frac{1}{2}\rho_t u_c^2 + R_t = \frac{D_0^2}{D_c^2}\left[\frac{1}{2}\rho_p (v_p - u)^2 + Y_p\right] = \frac{D_0^2}{D_c^2}\left[\frac{1}{2}\rho_t u^2 + R_t\right] \tag{29}$$

Namely,

$$u_c = \sqrt{\frac{A}{D_c^2} - B} \tag{30}$$

where $A = \frac{[\rho_p (v_p - u)^2 + 2Y_p]}{\rho_t} D_0^2 = \frac{[\rho_t u^2 + 2R_t]}{\rho_t} D_0^2$, and $B = \frac{2R_t}{\rho_t}$. When u_c = 0, the crater diameter D_c reaches the maximum value D_{cmax}.

$$D_{cmax} = \sqrt{\frac{A}{B}} \tag{31}$$

2.2.4 Penetration depth

To evaluate the penetration depth, the penetration process is assumed to: (1) occur immediately when the first particle of the projectile impacts the target, (2) reach the steady state instantaneously, and (3) finish when the last particle of the projectile impacts the target [33]. The penetration duration is calculated by $t = L_0/(v_p - u)$, where L_0 is the undeformed length of the projectile. The penetration depth P_{DOP} is the distance that the interface moves into the target.

$$P_{\mathrm{DOP}} = ut = \frac{uL_0}{v_{\mathrm{p}} - u} = \frac{1 - \sqrt{\rho_{\mathrm{t}}/\rho_{\mathrm{p}} + \left(1 - \rho_{\mathrm{t}}/\rho_{\mathrm{p}}\right)\dfrac{2\left(R_{\mathrm{t}} - Y_{\mathrm{p}}\right)}{\rho_{\mathrm{p}} v_{\mathrm{p}}^2}}}{-\dfrac{\rho_{\mathrm{t}}}{\rho_{\mathrm{p}}} + \sqrt{\rho_{\mathrm{t}}/\rho_{\mathrm{p}} + \left(1 - \rho_{\mathrm{t}}/\rho_{\mathrm{p}}\right)\dfrac{2\left(R_{\mathrm{t}} - Y_{\mathrm{p}}\right)}{\rho_{\mathrm{p}} v_{\mathrm{p}}^2}}} L_0 \quad (32)$$

3 Validation of the modified model

To validate the modified analytical model, .the predicted penetration velocity is compared to the available data in the literature by: experimental measurements of alumina targets [15] and finite element (FE) simulation of boron carbide targets [38]. In one literature [15], the penetration experiment of the alumina target subjected to the tungsten projectile impact was performed in a 38 mm launch tube two-stage light gas gun system. The target diameter was more than 30 times the projectile diameter. The initial impact velocity of the projectile ranged from v_{p} = 1.5 to 3.5 km s^{-1}. The radiography was conducted to measure both the impact velocity and the penetration velocity. In the other literature [38], an FE model using the AUTODYN-2D code was developed to simulate the penetration response of the boron carbide target impacted by the tungsten projectile. The Johnson-Holmquist constitutive formulation was used to describe the dynamic behaviour of the target. The material properties of the target and projectile obtained from the experiments and FE simulation (Table 1) were used to calculate the penetration variables using the model developed in Section 2.

The predicted penetration velocity *u* was compared to the experimental results of alumina [15] (Fig. 3) and the FE predictions of boron carbide [38] (Fig. 4). The use of

material degradation by the damage evolution parameter k in the model results in a more accurate analytical predictions. The model without damage (i.e., $k = 0$) under-predicts the penetration velocity, especially for the impact process of a tungsten projectile into the boron carbide target. When material degradation is incorporated, the deviation is less than 2–3% from the experimental and FE simulation results. In particular, the deviation is even smaller (<1%) at higher impact velocity range. The present model integrating the parameter k can accurately predict the two scenarios in the literature [15, 38]. However, future work on penetration experiments in a wide range of conditions (e.g., materials, impact velocities) is required to further validate the developed model.

The penetration process can also be predicted by other computational models, such as dual-horizon peridynamics [41, 42] and cracking particle method [43, 44]. These models characterise various complex physical phenomena during the penetration. The analytical model developed here does not directly describe the fracture process (crack initiation and propagation) of the ceramic target. Instead, the complex penetration behaviour is analytically quantified as a function of material properties that can be experimentally determined. In particular, a simple scalar is used to represent the damage evolution at high rates. The developed approach of analytical modelling is more computationally-efficient.

4 Results and discussion

The penetration behaviour is intrinsically dependent on the properties of materials including the projectile and the target, and extrinsically on the loading conditions such as the initial projectile impact velocity. Parametric modelling was performed by re-running the model as a function of these factors to evaluate their effects. The baseline model was based on the alumina target and the tungsten projectile in the experiment literature [15] (Table 1).

4.1 Penetration resistance of the ceramic target

4.1.1 Effect of material properties – k, Y_t and σ_f

Eq. (23) reveals that the penetration resistance is determined by material properties including the modulus degradation due to the damage evolution. The penetration resistance of alumina targets is predicted as a function of the compressive strength (Fig. 5), the tensile strength (Fig. 6) and the damage evolution (Figs. 5 and 6). A lower damage evolution parameter *k* suggests that the material is tougher and less degraded during the penetration. The lower *k* results in a higher penetration resistance (Figs. 5 and 6). For ceramic targets of higher dynamic compressive strength (e.g., Y_t = 3000 or 5000 MPa in Fig. 5) or lower tensile strength (σ_f = 200 or 462 MPa in Fig. 6), the penetration resistance is significantly affected by the material degradation property. It is thus difficult to penetrate a target if the damage evolves slowly (i.e., low *k*). However, the penetration resistance is less sensitive to the degradation of

materials if the compressive strength is low (e.g., Y_t = 1000 MPa) or the tensile strength is high (σ_f = 1000 MPa).

There is a transition damage evolution parameter $k_t \approx 4.0$ (Fig. 5). Below k_t, the target material is toughened and can decelerate the projectile efficiently; and the penetration resistance increases with the dynamic compressive strength. In contrast, for high $k > k_t$, an enhanced compressive strength reduces the resistance to penetration. The penetration resistance increases with the tensile strength of the target material regardless of its damage evolution behaviour (Fig. 6). However, if the material is highly toughened with $k \rightarrow 0$, the resistance becomes less sensitive to the tensile strength.

4.1.2 Selection of ceramic targets for penetration resistance

The material properties including degradation behaviour by damage evolution k are determined by the manufacturing process. Toughening process to lowering k can improve the penetration resistance; but toughening often sacrifices other material properties [45-47], e.g., reducing dynamic compressive strength of ceramics which can conversely decrease the penetration resistance (Fig. 5). The process to increase the tensile strength for penetration is probably not feasible, because the resistance is less dependent on the tensile strength when $k \rightarrow 0$ (Fig. 6) and also such a strengthening process is usually challenging for ceramic materials. Therefore, to improve the penetration resistance, a ceramic material that is toughened to hinder

crack propagation (damage evolution) is preferred over the material that is strengthened in compression/tension.

4.2 Penetration velocity

4.2.1 Effect of projectile properties and initial impact velocity

Fig. 7 reveals that the projectile density has a significant impact on the penetration velocity, while the effect of the projectile compressive strength is relatively trivial especially at the higher impact velocity (e.g., v_p >2 km s^{-1}). The penetration velocity increases with the initial impact velocity of the projectile. However, there is a critical initial impact velocity below which the penetration cannot occur. This critical velocity decreases as the projectile density increases; the compressive strength has a similar effect on the critical velocity but to a much less extent. Thus lighter projectile requires higher initial impact velocity to enable the penetration process. This suggests that heavier (and secondly stronger) projectile materials should be selected for armour-piercing capability in wartime.

4.2.2 Effect of target material properties especially at low impact velocities

If the projectile is launched at the very high initial impact velocity v_p, the second term in the square root part in Eq. (25) can be neglected. Thus the penetration velocity u is predominantly determined by the projectile velocity v_p and the densities of the projectile and target (ρ_p, ρ_t). At high impact velocity e.g., v_p = 5 km s^{-1} as shown in Figs. 8 and 9, the target material properties such as the compressive strength Y_t, the

tensile strengths σ_f and the degradation parameter k have little influence on the penetration velocity. However, at the low impact velocity (e.g., v_p = 1 km s^{-1} in Figs. 8 and 9), the penetration velocity becomes significantly dependent on the properties (Y_t, σ_f and k) of the ceramic target through the penetration resistance R_t in Eq. (25). The penetration velocity substantially increases with the damage evolution parameter k especially in ceramic targets with higher Y_t (e.g., 5000 MPa in Fig. 8) and lower σ_f (e.g., 200 MPa in Fig. 9).

Unlike other mechanical properties (e.g., Y_t, σ_f), it is usually challenging to obtain the accurate value of the damage evolution scalar k. Therefore, the uncertainty of k can have an impact on the accuracy of the analytical prediction (e.g., R_t and u), especially for higher Y_t or lower σ_f.

4.3 Crater diameter and penetration depth

The depth of penetration and the diameter of the resultant crater are the two parameters to evaluate the performance of various armour ceramic target materials impacted by a long rod projectile. An increase in crater diameter and penetration depth suggests a higher possibility to damage the objects behind the target. The crater diameter D_{cmax} (Fig. 10) and the penetration depth P_{DOP} (Fig. 11) were calculated as a function of the projectile velocity v_p and the damage evolution parameter k. The D_{cmax} and P_{DOP} were then normalised by the original projectile diameter D_0 and length L_0, respectively.

During the penetration process, the stress around the cavity may not be high enough to squeeze the target material out of the projectile path. Therefore, the crater diameter almost remains equal to the projectile diameter at lower impact velocities (e.g. $v_p < 1.2$ km s^{-1}) as shown in Fig. 10. However, at higher velocities (e.g., $v_p >$ 2 km s^{-1}), the crater diameter increases approximately linearly with the impact velocity. Penetration occurs only when the impact velocity exceeds the critical value as discussed in Section 4.2.1 (refer to Fig. 7). This critical impact velocity also applies to the depth of penetration (Fig. 11). The depth P_{DOP} increases significantly with the low impact velocity. But at the high velocity it tends to approach a constant that can be estimated in the hydrodynamic condition (i.e., zero strengths for both the target and projectile materials).

The material degradation with a higher k during penetration leads to the increased crater diameter and penetration depth (Figs. 10 and 11). This suggests that the brittle material can be easily comminuted radially under the long rod projectile impact. The damage evolution affects the crater diameter more substantially at higher impact velocities than at lower velocities, whilst its effect on the penetration depth is significant at lower velocities.

5 Conclusions

A modified analytical model to determine the penetration behaviour of a ceramic target impacted by a long rod projectile was developed based on the spherical cavity

expansion model. The elastic modulus degradation characterised by the damage evolution parameter k was incorporated into the model. The conclusions were drawn as follows.

- The model validated by the experimental and numerical data in the literature can predict the penetration process more accurately compared to the model without considering the damage evolution.
- The penetration resistance of ceramic targets is significantly affected by the damage evolution, especially in the ceramic of higher dynamic compressive strength Y_t and lower tensile strength σ_f. For tougher ceramics with the k below the transition value, the target resistance increases with both Y_t and σ_f, but becomes less sensitive to σ_f when $k \rightarrow 0$. Toughening process to minimise the damage evolution (lower k) is preferred over strengthening process in order to improve the target resistance.
- The penetration velocity is predominantly determined by the initial projectile impact velocity and the densities of the projectile and target. But at the lower impact velocity, it is also influenced by the target properties such as k, Y_t and σ_f. Both the crater diameter and penetration depth increases with the impact velocity and the damage evolution parameter.

Acknowledgements

The authors gratefully acknowledge the financial support of the National Natural Science Foundation of China (11802028), the China Postdoctoral Science Foundation Grant (2019M650502) and the Academic Research Fund (AcRF) Tier 1 by Ministry of Education in Singapore. ZW also thanks the Nanyang Technological University (NTU) Research Student Scholarship for his PhD study during which this work was carried out.

References

[1] R.Q. Chi, A. Serjouei, I. Sridhar, G.E.B. Tan, Ballistic impact on bi-layer alumina/aluminium armor: A semi-analytical approach, Int. J. Impact Eng., 52 (2013) 37-46.

[2] J.D. Clayton, Modeling and simulation of ballistic penetration of ceramic-polymer-metal layered systems, Mathematical Problems in Engineering, (2015).

[3] J.D. Clayton, R.H. Kraft, R.B. Leavy, Mesoscale modeling of nonlinear elasticity and fracture in ceramic polycrystals under dynamic shear and compression, Int. J. Solids Struct., 49 (2012) 2686-2702.

[4] I.G. Crouch, G. Appleby-Thomas, P.J. Hazell, A study of the penetration behaviour of mild-steel-cored ammunition against boron carbide ceramic armours, Int. J. Impact Eng., 80 (2015) 203-211.

[5] Z. Wang, P. Li, Dynamic failure and fracture mechanism in alumina ceramics: Experimental observations and finite element modelling, Ceram. Int., 41 (2015) 12763-12772.

[6] Z. Wang, P. Li, W. Song, Inelastic deformation micromechanism and modified fragmentation model for silicon carbide under dynamic compression, Mater. Des., 157 (2018) 244-250.

[7] C.E. Anderson, D.L. Littlefield, J.D. Walker, Long-rod penetration, target resistance, and hypervelocity impact, Int. J. Impact Eng., 14 (1993) 1-12.

[8] C.E. Anderson, D.L. Orphal, Analysis of the terminal phase of penetration, Int. J. Impact Eng., 29 (2003) 69-80.

[9] M.R. Aziz, W. Kuntjoro, N.V. David, Terminal Ballistic of Aluminium Plate: An Experiment and Numerical Simulation, in: M. Abdullah, Y.H. Min, N.A.M. Bashar, S. Nasir (Eds.) International Conference on Advanced Science, Engineering and Technology, Amer Inst Physics, Melville, 2016.

[10] D.R. Curran, L. Seaman, T. Cooper, D.A. Shockey, Micromechanical model for comminution and granular flow of brittle material under high-strain rate application to penetration of ceramic targets, Int. J. Impact Eng., 13 (1993) 53-83.

[11] S.N. Perevislov, I.A. Bespalov, Impact-resistant silicon-carbide-based ceramic materials, Technical Physics Letters, 43 (2017) 720-722.

[12] A. Rashed, M. Yazdani, A.A. Babaluo, P.H. Parvin, Investigation on high-velocity impact performance of multi-layered alumina ceramic armors with polymeric interlayers, J. Compos. Mater., 50 (2016) 3561-3576.

[13] S. Satapathy, S. Bless, Calculation of penetration resistance of brittle materials using spherical cavity expansion analysis, Mech. Mater., 23 (1996) 323-330.

[14] S.S. Satapathy, S.J. Bless, Cavity expansion resistance of brittle materials obeying a two-curve pressure-shear behavior, J. Appl. Phys., 88 (2000) 4004-4012.

[15] R. Subramanian, S.J. Bless, Penetration of semi-infinite AD995 alumina targets by tungsten long rod penetrators from 1.5 to 3.5 km/s, Int. J. Impact Eng., 17 (1995) 807-816.

[16] Z. Wang, P. Li, Characterisation of dynamic behaviour of alumina ceramics: evaluation of stress uniformity, AIP Adv., 5 (2015) 16.

[17] C. Denoual, F. Hild, A damage model for the dynamic fragmentation of brittle solids, Comput. Methods Appl. Mech. Eng., 183 (2000) 247-258.

[18] B.A. Gailly, H.D. Espinosa, Modelling of failure mode transition in ballistic penetration with a continuum model describing microcracking and flow of pulverized media, Int. J. Numer. Methods Eng., 54 (2002) 365-398.

[19] R.B. Leavy, R.M. Brannon, O.E. Strack, The Use of Sphere Indentation Experiments to Characterize Ceramic Damage Models, Int. J. Appl. Ceram. Technol., 7 (2010) 606-615.

[20] N.K. Naik, S. Kumar, D. Ratnaveer, M. Joshi, K. Akella, An energy-based model for ballistic impact analysis of ceramic-composite armors, International Journal of Damage Mechanics, 22 (2013) 145-187.

[21] D. Ray, R.M. Flinders, A. Anderson, R.A. Cutler, J. Campbell, J.W. Adams, Effect of microstructure and mechanical properties on the ballistic performance of sic-based ceramics, in: L.P. Franks, A. Wereszczak, E. LaraCurzio (Eds.) Advances in Ceramic Armor Ii, Amer Ceramic Soc, Westerville, 2007, pp. 85-96.

[22] D.A. Shockey, A.H. Marchand, S.R. Skaggs, G.E. Cort, M.W. Burkett, R. Parker, Failure phenomenology of confined ceramic targets and impacting rods, Int. J. Impact Eng., 9 (1990) 263-275.

[23] J. Sternberg, Material properties determining the resistance of ceramics to high-velocity penetration, J. Appl. Phys., 65 (1989) 3417-3424.

[24] H.N.G. Wadley, M.R. O'Masta, K.P. Dharmasena, B.G. Compton, E.A. Gamble, F.W. Zok, Effect of core topology on projectile penetration in hybrid aluminum/alumina sandwich structures, Int. J. Impact Eng., 62 (2013) 99-113.

[25] D.L. Orphal, R.R. Franzen, A.J. Piekutowski, M.J. Forrestal, Penetration of confined aluminum nitride targets by tungsten long rods at 1.5-4.5 km/s, Int. J. Impact Eng., 18 (1996) 355-368.

[26] C.E. Anderson, T. Behner, T.J. Holmquist, D.L. Orphal, Penetration response of silicon carbide as a function of impact velocity, Int. J. Impact Eng., 38 (2011) 892-899.

[27] T. Behner, C.E. Anderson, T.J. Holmquist, D.L. Orphal, M. Wickert, D.W. Templeton, Penetration dynamics and interface defeat capability of silicon carbide against long rod impact, Int. J. Impact Eng., 38 (2011) 419-425.

[28] W. Herrmann, J.S. Wilbeck, Review of hypervelocity penetration theories, Int. J. Impact Eng., 5 (1987) 307-322.

[29] J.G. Ning, H.L. Ren, T.T. Guo, P. Li, Dynamic response of alumina ceramics impacted by long tungsten projectile, Int. J. Impact Eng., 62 (2013) 60-74.

[30] A. Tate, A theory for the deceleration of long rods after impact, J. Mech. Phys. Solids, 15 (1967) 387-399.

[31] R.F. Recht, Taylor ballistic impact modelling applied to deformation and mass loss determinations, Int. J. Eng. Sci., 16 (1978) 809-827.

[32] R.L. Woodward, A simple one-dimensional approach to modeling ceramic composite armor defeat, Int. J. Impact Eng., 9 (1990) 455-474.

[33] C.E. Anderson, D.L. Orphal, An examination of deviations from hydrodynamic penetration theory, Int. J. Impact Eng., 35 (2008) 1386-1392.

[34] C.E. Anderson, J.P. Riegel, A penetration model for metallic targets based on experimental data, Int. J. Impact Eng., 80 (2015) 24-35.

[35] S. Feli, M.H. Yas, M.R. Asgari, An analytical model for perforation of ceramic/multi-layered planar woven fabric targets by blunt projectiles, Compos. Struct., 93 (2011) 548-556.

[36] C.S. Lin, Y.L. Chen, High velocity impact of projectiles on ceramic and metal dual layer target panels, Journal of Mechanics, 28 (2012) 499-506.

[37] J.D. Walker, Analytically modeling hypervelocity penetration of thick ceramic targets, Int. J. Impact Eng., 29 (2003) 747-755.

[38] L. Westerling, P. Lundberg, B. Lundberg, Tungsten long-rod penetration into confined cylinders of boron carbide at and above ordnance velocities, Int. J. Impact Eng., 25 (2001) 703-714.

[39] F. Collombet, J.Y. Tranchet, Damage behavior of alumina submitted to a divergent spherical wave, J. Phys. IV, 4 (1994) 641-646.

[40] M.J. Forrestal, D.B. Longcope, Target strength of ceramic materials for high-velocity penetration, J. Appl. Phys., 67 (1990) 3669-3672.

[41] H.L. Ren, X.Y. Zhuang, Y.C. Cai, T. Rabczuk, Dual-horizon peridynamics, Int. J. Numer. Methods Eng., 108 (2016) 1451-1476.

[42] H.L. Ren, X.Y. Zhuang, T. Rabczuk, Dual-horizon peridynamics: A stable solution to varying horizons, Comput. Methods Appl. Mech. Eng., 318 (2017) 762-782.

[43] T. Rabczuk, T. Belytschko, Cracking particles: a simplified meshfree method for arbitrary evolving cracks, Int. J. Numer. Methods Eng., 61 (2004) 2316-2343.

[44] T. Rabczuk, T. Belytschko, A three-dimensional large deformation meshfree method for arbitrary evolving cracks, Comput. Methods Appl. Mech. Eng., 196 (2007) 2777-2799.

[45] P. Badica, D. Batalu, M. Burdusel, M.A. Grigoroscuta, G.V. Aldica, M. Enculescu, R.A. Gabor, Z.Y. Wang, R.X. Huang, P.F. Li, Compressive properties of pristine and SiC-Te-added MgB2 powders, green compacts and spark-plasma-sintered bulks, Ceram. Int., 44 (2018) 10181-10191.

[46] P. Badica, S. Grasso, H. Borodianska, S.S. Xie, P.F. Li, P. Tatarko, M.J. Reece, Y. Sakka, O. Vasylkiv, Tough and dense boron carbide obtained by high-pressure (300 MPa) and low-temperature (1600 degrees C) spark plasma sintering, J. Ceram. Soc. Jpn., 122 (2014) 271-275.

[47] P. Badica, H. Borodianska, S.M. Xie, T. Zhao, D. Demirskyi, P.F. Li, A.I.Y. Tok, Y. Sakka, O. Vasylkiv, Toughness control of boron carbide obtained by spark plasma sintering in nitrogen atmosphere, Ceram. Int., 40 (2014) 3053-3061.

List of Symbols

Symbol	Definition
For the target	
a	Radius to the comminuted/cracked interface
b	Radius to the elastic/intact interface
c	Radius to the cracked/elastic interface
h	Radius to the cavity/comminuted interface
p_0	Initial stagnation pressure
u_c	Crater growth velocity in the radial direction
u_r	Radial displacement
D	Damage scalar
D_c	Crater diameter
D_{cmax}	Maximum crater diameter
E	Initial elastic modulus
E_D	Degraded elastic modulus
P_{hyd}	Hydrostatic pressure
P_{DOP}	Depth of penetration
R_t	Penetration resistance (also called target resistance)
Y_t	Dynamic compressive strength of the target
ε_r	Radial strain
ε_θ	Hoop strain
λ_l	Hydrostatic pressure-shear coefficient
μ	Normal stress to shear stress coefficient
ν	Poisson's ratio
ρ_t	Density of the target
σ_f	Tensile strength of the target
σ_r	Radial stress
σ_θ	Hoop stress
τ	Shear stress
For the projectile	
u	Penetration velocity at the projectile/target interface
v_P	Initial impact velocity of the projectile
D_0	Diameter of the projectile
L_0	Original length of the projectile
Y_P	Dynamic strength of the projectile
ρ_P	Density of the projectile

List of Tables

Table 1 Material properties of the ceramic target and the projectile in the penetration experiment and numerical simulation in the literature.

Parameter	Experimental literature [15]		Numerical literature [38]	
	Target	Projectile	Target	Projectile
	Alumina	Tungsten	Boron carbide	Tungsten
Density (kg m^{-3}), ρ	3890	19300	2550	17600
Young's modulus (GPa), E	390	-	461	-
Poisson's ratio, v	0.24	-	0.17	-
Tensile strength (MPa), σ_f	462	-	260	-
Compressive strength (MPa), Y	3000	2452	3000	2000
Damage evolution parameter, k *	1.0	-	1.2	-

* The damage evolution parameter was assumed in this study.

List of Figures

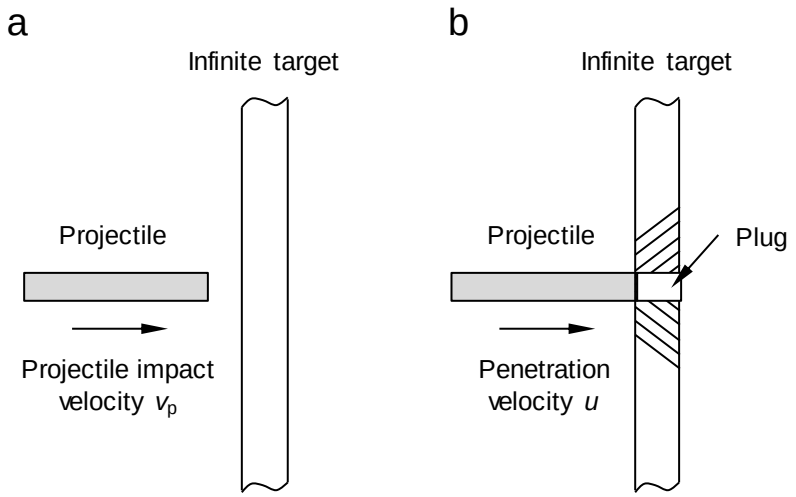

Figure 1: Sequence of a long projectile impacting on an infinite ceramic target: (a) before penetration and (b) onset of penetration.

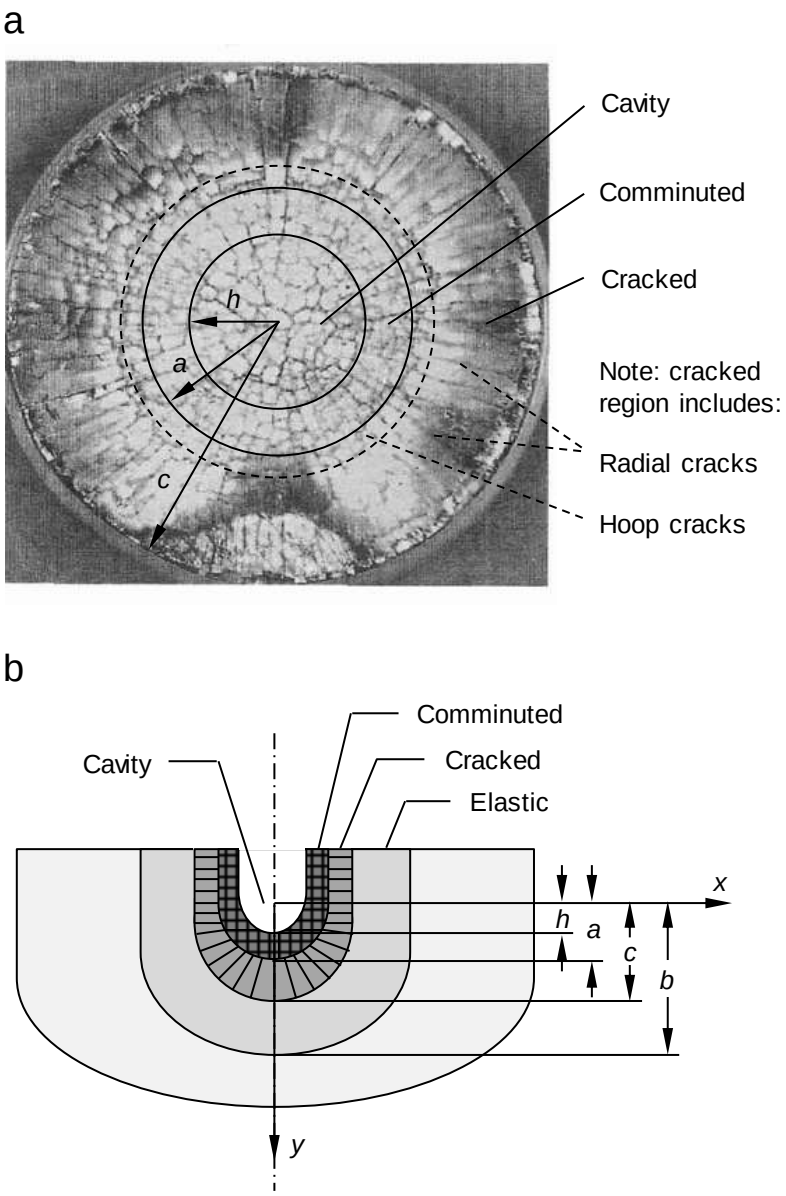

Figure 2: (a) A ceramic target specimen recovered from the long projectile impact testing [39], and (b) the schematic of the response regions in the ceramic target after penetration.

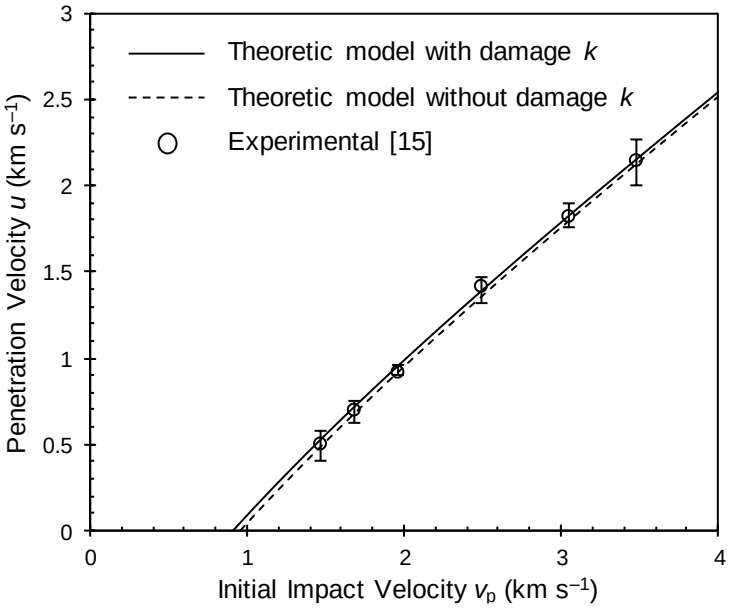

Figure 3: Comparison between the theoretic prediction and the experimental measurement [15] of the penetration velocity in an alumina target subjected to the tungsten projectile impact with different initial velocities.

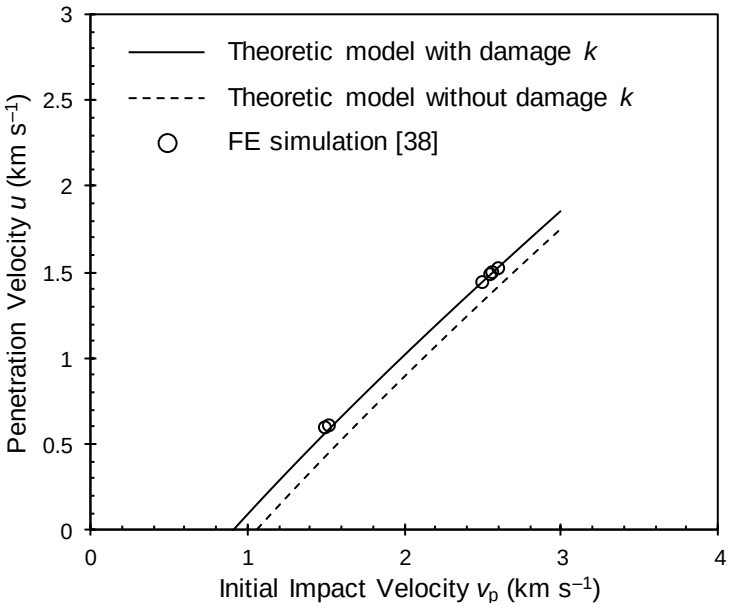

Figure 4: Comparison between the theoretic prediction and the finite element simulation [38] of the penetration velocity in a boron carbide target subjected to the tungsten projectile impact with different initial velocities.

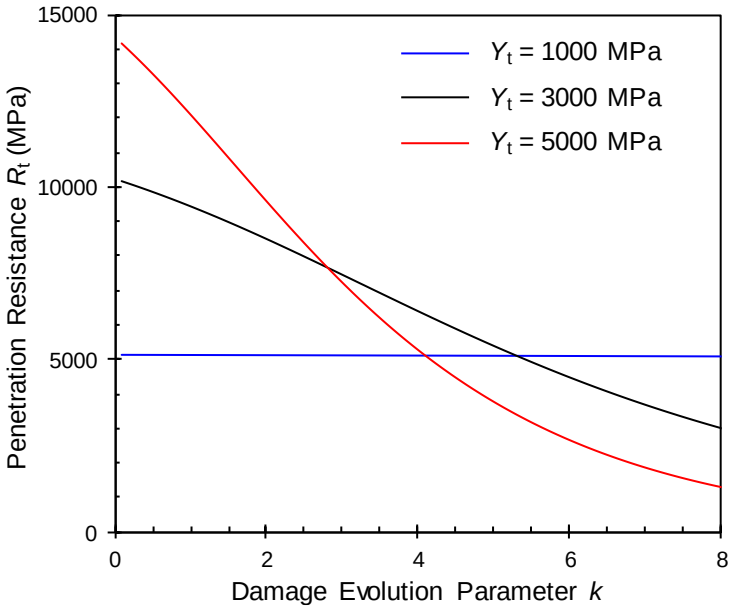

Figure 5: Effect of the compressive strength and damage evolution parameter of a ceramic target on its penetration resistance.

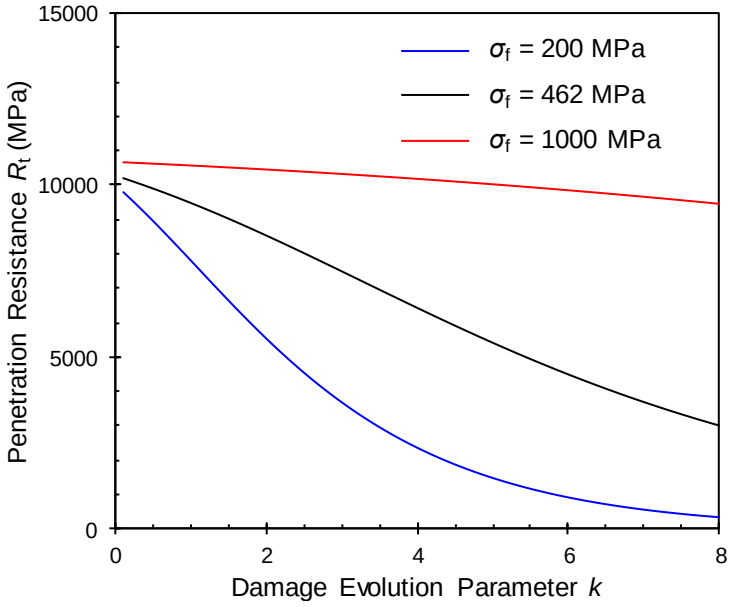

Figure 6: Effect of the tensile strength and damage evolution parameter of a ceramic target on its penetration resistance.

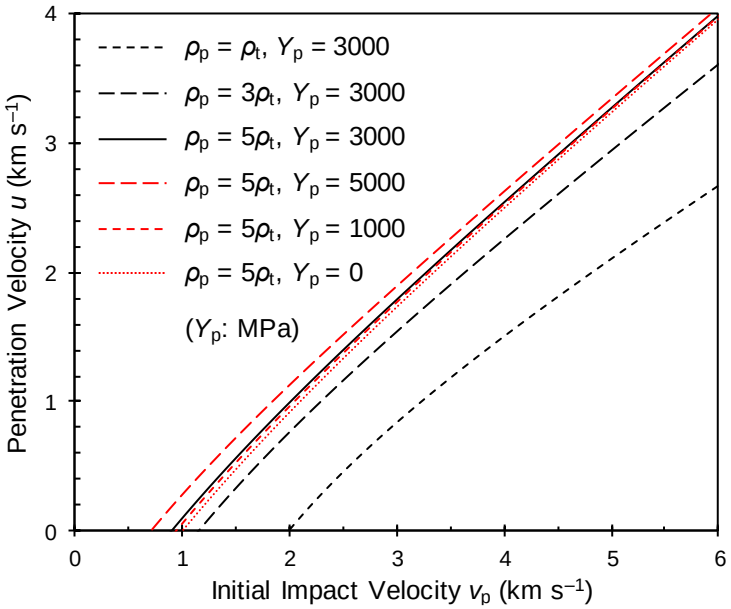

Figure 7: Penetration velocity as a function of the density, dynamic compressive strength and initial impact velocity of the projectile.

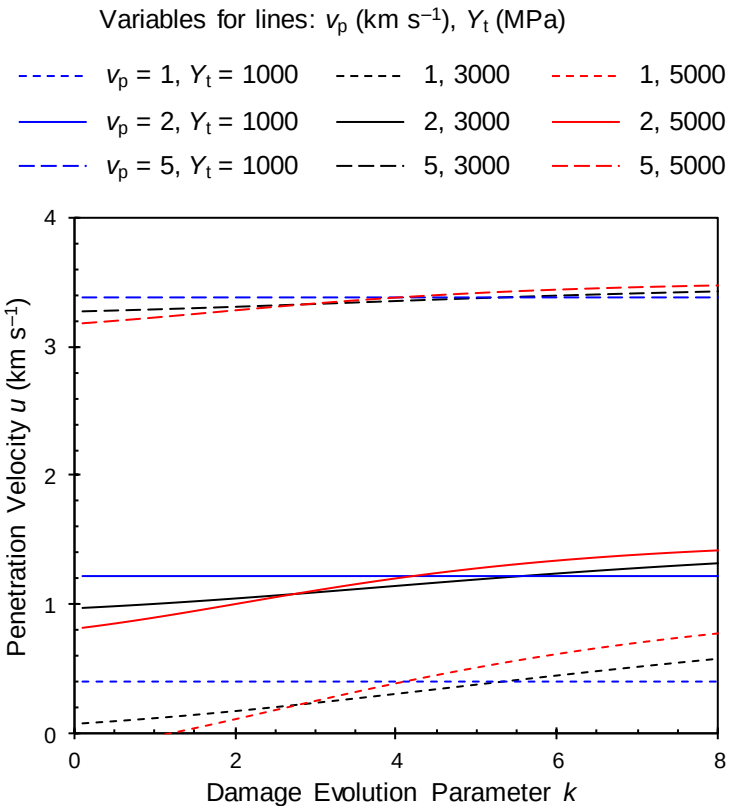

Figure 8: Penetration velocity as a function of the compressive strength and damage evolution parameter of a ceramic target at three different projectile impact velocities.

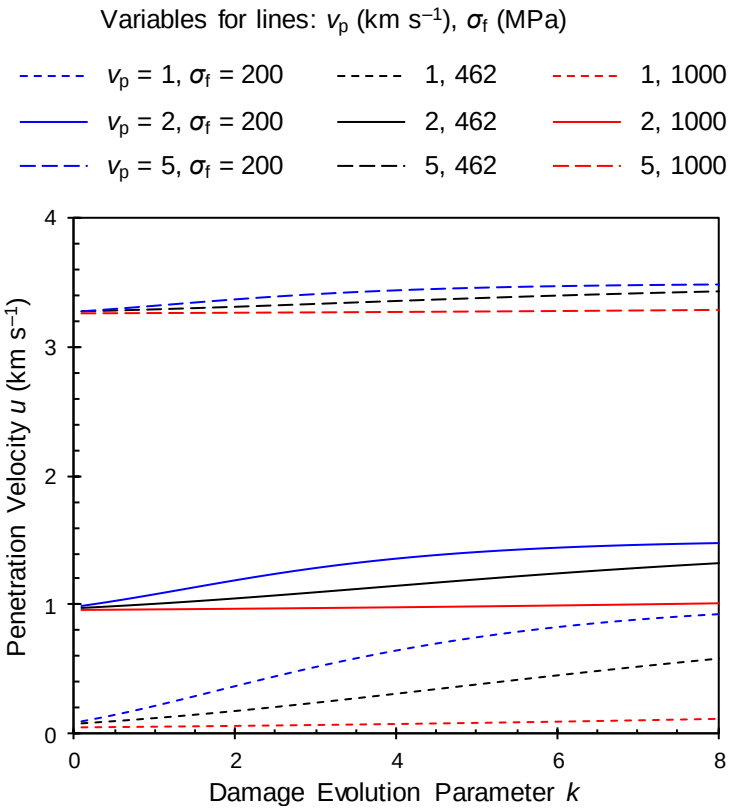

Figure 9: Penetration velocity as a function of the tensile strength and damage evolution parameter of a ceramic target at three different projectile impact velocities.

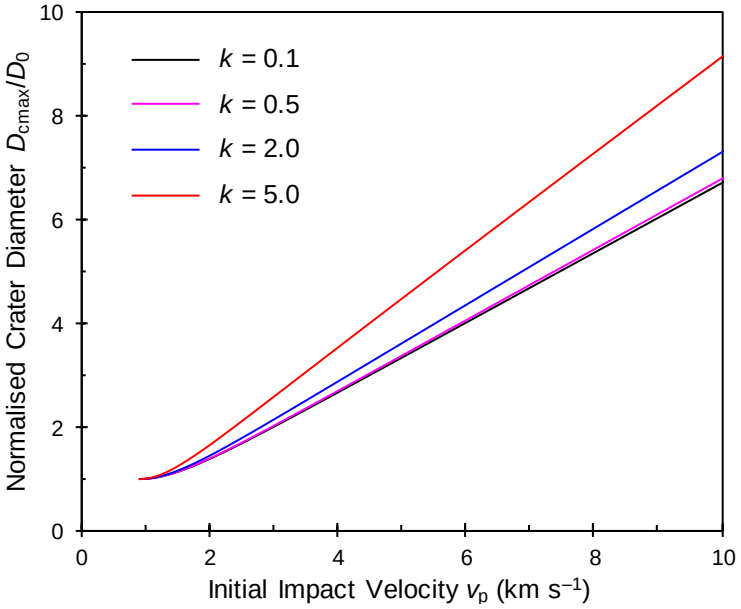

Figure 10: Effect of the damage evolution parameter on the crater diameter.

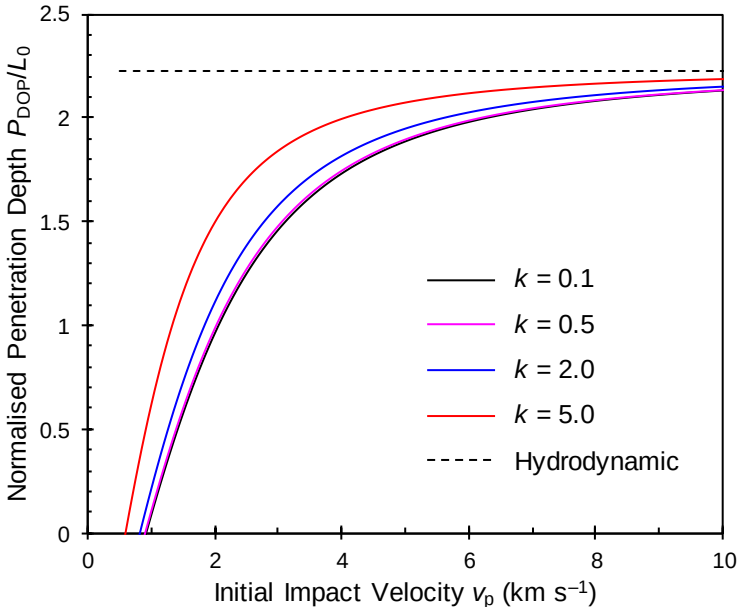

Figure 11: Effect of the damage evolution parameter on the penetration depth.